Diyala Journal for Pure Science

Synthesis and Characterization of Magnetic (Co-Ni-Fe2O4) Nano Ferrite for Biomedical Application

Marwa H. Sabbar*, T. H. Mubarak and Nada S. Ahmad

Department of Physics – College of Science – University of Diyala,

am6645849@gmail.com

Received: 1 June 2022 **Accepted: 27 July 2022**

DOI: https://dx.doi.org/10.24237/djps.1804.600C

Abstract

In this research, prepared the samples in formal $Co_{1-x}Ni_xFe_2O_4$ ferrites nanoparticles when x, (x = 0.0, 0.2, and 0.4), by two methods, Co – precipitation and pulsed laser deposition (PLD). Samples prepared using Co-precipitation was calcined in (300 °C). The resulting powder is then compressed into a disc with a diameter of (2 cm) and then we use laser deposition technology to obtain thin film. The x-ray spectrum shows that the pattern of the particles formed is of the face -centered cubic and the theoretical values of the lattice constant and and crystalline size (D) are calculated The crystalline size calculated is located in the range (22.6-26.6 nm), either in the pulsed laser deposition method in the range (13.7-13.7nm), which reflects the highly crystalline nature of these nanoparticles.. The FTIR spectrum shows two absorption bands ranging between 400 and 600 cm^{-1}. These bands indicate that the composition of the spectrum for all the samples is ferrite. The Field emission scanning electron microscopes (FE-SEM) images confirmed that the preparation methods produced spherical nanoparticles with a slight change in the particle size distribution. The average particle size by coprecipitation had estimated to be about 23 nm and the average particle size by pulsed laser deposition (PLD) method had estimated to be about 20 nm. The magnetic properties vibrating sample magnetometer (VSM) had a good correlation with the structural parameters of the spinal structure, which increased with the Ni content. Both of samples for powder and (PLD) have

Diyala Journal for Pure Science

Synthesis and Characterization of Magnetic (Co-Ni-Fe2O4) Nano Ferrite for Biomedical Application

Marwa H. Sabbar, T. H. Mubarak and Nada S. Ahmad

been show S shape of hysterias loop. When using nanoparticles prepared by using the method of co-precipitation on Escherichia coli (S.aureus) bacteria, and Streptococcus bacteria,, it was found that highest inhibition zone ranged from (27-33) mm. When using nanoparticles prepared by using the method of pulsd laser deposition on the same types of bacteria, (S.aureus)was found to have the highest inhibition zone (22-32) mm.

Keywords: Co-Ni-Fe_2O_4 ferrites, magnetic nanoparticles, Co-precipitation method, antibacterial activity for ferrite.

توليف وتوصيف الفريت النانوي المغناطيسي (Co-Ni-Fe2O4) للتطبيقات الطبية الحيوية

مروه حازم صبار، تحسين حسين مبارك وندى سهيل احمد[1]

قسم الفيزياء – كلية العلوم – جامعة ديالى

الخلاصة

تم في هذا البحث تحضير عينات الفيرايت النانوية بصيغة $Co_{1-x}Ni_xFe_2O_4$ عندما(X=0.0,0.2,0.4) بواسطة طريقتان الترسيب المشترك والترسيب بالليزر النبضي العينات التي حضرت بطريقة الترسيب المشرك لدنت بدرجة حرارة 300 درجة سليزية، ثم بعد ذلك ضغط المسحوق ليحول الى قرص (2) سم لغرض تشعيعه بطاقة ليزر 600 ملي جول لتحسين بعض خواص المسحوق درست الخواص التركيبة والمغناطيسية باستخدام حيود الاشعة السينية وقياس المغناطيسية لاهتزاز العينة. يُظهر طيف الأشعة السينية أن نمط الجسيمات المتكونة هو النمط المكعب المتمركز الأوجه وتم حساب القيم النظرية لثابت الشبيكة، والحجم البلوري D حيث يقع الحجم البلوري المحسوب في المدى (22.6-25.2 نانومتر)، إما في طريقة الترسيب بالليزر النبضي في المدى (13.4-13.7 نانومتر). تُظهر تحويلات فورير لمطيافية الأشعة تحت الحمراء FTIR وجود حزمتي أمتصاص تتراوح ضمن المدى 400 – 600 سم$^{-1}$. تشير هذه الحزم أن تركيب الطيف لجميع النماذج هو الفيرايت. أكد فحص (FE-SEM) أن طرق التحضير أنتجت جسيمات نانوية كروية مع تغيير طفيف في توزيع حجم الجسيمات. يقدر متوسط حجم الجسيمات بواسطة الترسيب المشترك بحوالي 23 نانومتر ومتوسط حجم الجسيمات عن طريق طريقة الترسيب بالليزر النبضي (PLD) يقدر بحوالي 20 نانومتر.

Diyala Journal for Pure Science

Synthesis and Characterization of Magnetic (Co-Ni-Fe2O4) Nano Ferrite for Biomedical Application

Marwa H. Sabbar, T. H. Mubarak and Nada S. Ahmad

اظهرت نتائج قياس المغناطسية لاهتزاز العينة (VSM) ان للخصائص المغناطيسيه علاقة جيدة مع المعلمات الهيكلية للبنية الاسبنل ، والتي زادت مع محتوى النيكل,أظهرت كل من عينات الباودر و (PLD) شكل S في حلقة التخلف المغناطيسي. بعض العينات اضهرت سلوك مواد فائقة المغناطيسية.عند أستخدام الجسيمات النانوية المحضرة بطريقه الترسيب المشترك على انواع من البكتريا بكتريا الـ *Escherichia coli S.aureus bacteria bacteria*, وُجد أن اعلى نطاق التثبيط لبكتريا الـ S.aureus bacteriaتراوح ضمن 27 – 33 ملم. اما عند استخدام الجسيمات النانوية المحضرة بطريقه الترسيب بالليزر النبضي على نفس الانواع من البكتريا وجد ان بكتريا (S.aureus bacteria) قد سجلت اعلى نسبة تثبيط تتراوح مابين(22-32ملم).

الكلمات المفتاحية: الكوبلت –نيكل فيرايت، الجسيمات النانوية المغناطيسية، تقنية الترسيب المشترك، فعالية المضادات البكتيرية للفيرايت.

Introduction

Spinel ferrite is the class of oxide materials with remarkable electrical and magnetic properties, which have been investigated and applied during the last few decades. Amongst all inverse spinel ferrites, the nickel substituted cobalt ferrite has been extensively studied in view of their good chemical and thermal stability, high electrical resistivity, magnetic anisotropy, high coercivity and moderate saturation magnetization, various exchange interactions and super-paramagnetism etc. In addition to these, they exhibit ferrimagnetism, originating from the magnetic moment of anti-parallel spins between Fe3+ ions at tetrahedral sites and Co^{2+} or Ni^{2+} ions at octahedral sites [1]. Due to the magnetic properties. Cobalt ferrite, CoFe2O4, is a well-known hard magnetic material [2]. Recently, Ni^{2+} ions were added to Co ferrite films to improve the magnetic.

Materials and Methods

Ferrite powders were prepared, cobalt nitrate, iron nitrate and nickel nitrate were used as starting materials.

Diyala Journal for Pure Science

Synthesis and Characterization of Magnetic (Co-Ni-Fe2O4) Nano Ferrite for Biomedical Application

Marwa H. Sabbar, T. H. Mubarak and Nada S. Ahmad

Table 1: Shows the raw materials and their density

Mol. Mass g. mol^-1	Chemical formula	Compounds
403.8	Fe $(NO_3)_3.9H_2O$	Iron nitrate
291.031	Co $(NO_3)_2.6H_2O$	Cobalt nitrate
290.79	$Ni(NO_3)_2.6H_2O$	nickel nitrate
39.9971	NaOH	Sodium hydroxide

Synthesis and Characterization

1. Co-precipitation Method

It was prepared by mixing the metal nitrates Co $(NO_3)_2.6H_2O$, Ni $(NO_3)_2.6H_2O$, and Fe $(NO3)_3.9H_2O$ in 100 mL of deionization water under constant stirring at 80 °C for 40 minutes. 100 mL deionization water to make the Co-Ni-Fe_2O_4 in order to create Co-Ni-Fe_2O_4 NCs (x = 0.0, 0.2, and 0.4), then add (NaOH) slowly to the mixture material until pH of the suspension is 12 and the color of the 'precipitation becomes brown. As highlighted the obtained solution was remained at all day to dry and its color goes from brown to black. the procurers calcined at 300 °C.

2. Calcinations and Pellet Formation

The resulting powder is placed in a ceramic pot and then roasted at 300 °C for 3 hours to remove reaction residues such as water or carbon dioxide molecules from combustion, resulting in the necessary ferrite powder. Then 0.5 g of burnt samples and samples that were concentration (x = 0.0, 0.2, 0.4) M a round pellets 2 cm in diameter and 3 mm thick. This is achieved by pressing 500 ton for five minutes with a hydraulic press using the dry-press method, as shown in figure (1).

Synthesis and Characterization of Magnetic (Co-Ni-Fe2O4) Nano Ferrite for Biomedical Application

Marwa H. Sabbar, T. H. Mubarak and Nada S. Ahmad

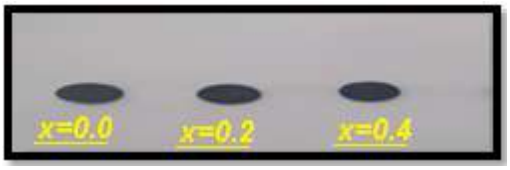

Figure 1: Transformation of powder to compact sample.

3. Pulsed Laser deposition (PLD) Method

Figure 2 shows the experimental setup for laser depostion of solid metal target by pulsed laser deposition.The pulsed laser deposition experiment was carried out inside a vacuum chamber generally in ($3*10^{-2}$Torr) vacuum conditions. The focused Nd: YAG laser beam at 600 mJ with a wave length radiation at 1064nm (pulse width 10 ns) repetition frequency (3 Hz), for 650 laser pulses incident on the target surface makes an angle of 45° with it. The distance between the target and the laser was set to (10 cm), and between the target and the substrate was (3cm).

Figure 2: Shows the pulsed laser deposition (PLD) technique.

Antibacterial activity of Co-Ni-Fe_2O_4 NCs ferrite

To determine whether or not Co-Ni-Fe_2O_4 ferrite nanoparticles had the ability to create a zone of inhibition in bacteria in a dose-dependent manner, bacterial cultures were established. In order to demonstrate bactericidal action, the Co-Ni-Fe_2O_4 ferrite must exhibit a wide zone of inhibition for gram-negative bacteria (E. coli) and a smaller zone of inhibition for gram-positive bacteria (S. aureus). Gram-negative bacteria have a distinct cell wall structure that distinguishes

them from their Gram-positive counterparts. Bacterial cells from the Gram-positive group are covered with a thick layer of peptidoglycan that contains lipopolysaccharide as well as phospholipids and proteins [3-4].

This test allows for the clear observation of the bactericidal action of the Co-Ni-Fe_2O_4 NCs that have been generated in the laboratory. In order to have a bactericidal effect, the thickness of the cell wall, the shape of the cell membrane, and the ability of the outermost membrane to inhibit the creation of reactive oxygen species (ROS) caused by the metal ions are all taken into consideration. Cell membrane damage, the generation of reactive oxygen species (ROS), DNA damage caused by aerobic respiration, and cell division are all examples of NPs' antimicrobial activity [3-4].

Because of their ability to penetrate cells' walls, Co-Ni-Fe_2O_4 NCs may cause cells to leak and exocytose, as well as inhibit the activity of essential enzymes. Using the following equation [5, 6], it has been possible to calculate the percentages of inhibitory zones:

$$\textbf{\textit{Inhibition Zone}}\ (\%) = \frac{\textbf{\textit{Diameter of the inhibition zone in mm}}}{\textbf{\textit{Diameter of pertiplate}}\ (\textbf{90 mm})} \times \textbf{100}\% \quad \text{.....(1)}$$

Result and Discussion

1. X-ray Diffraction (XRD) patterns of Co-Ni-Fe_2O_4 for co- precipitation method:

Figure 3 shows the XRD patterns of $Co_{1-x}Ni_xFe_2O_4$ powders prepared at different ratios by co-precipitation method and pressed at pellet. All samples had Face-center cubic structure for all of the patterns with diffraction peaks located at 2θ= 18.2650°, 30.0835°, 35.4434°, 36.5690°, 43.0812°, 53.4526°, 56.9633°, 62.5912°, 71.0062°, 74.0613°, 75.0529°, and 78.9280 identical with the standard diffracted lines from (111), (220), (311), (222), (400), (422), (511), (440), (620), (533), (622), and (444) planes, respectively, corresponding to Spinal phase. These peaks identical with standard JCPDS card no. 22-1086. Small additional peaks appeared in patterns corresponding to the Fe_2O_3 Hematite structure [7].

It seems that increasing the substitution levels of Ni instead of Co into the ferrite structures cause to slightly shifts in the peak's location toward higher angle, indicate on variation in lattice parameter due to the variation in ion radius. It can be seen that the crystallinity enhanced, and small variation in the lines broadening. This result agree with previous study [7], [8].

It is worth mentioning here that spinel ferrites MFe_2O_4 (where M is, Ni^{+2}, Co^{+2}, Zn^{2+}) is very similar in crystal structure with little difference in lattice dimensions. This makes these compounds have nearly similar X-ray diffraction patterns with a very small shift in the location of the diffraction peaks [7], [9].

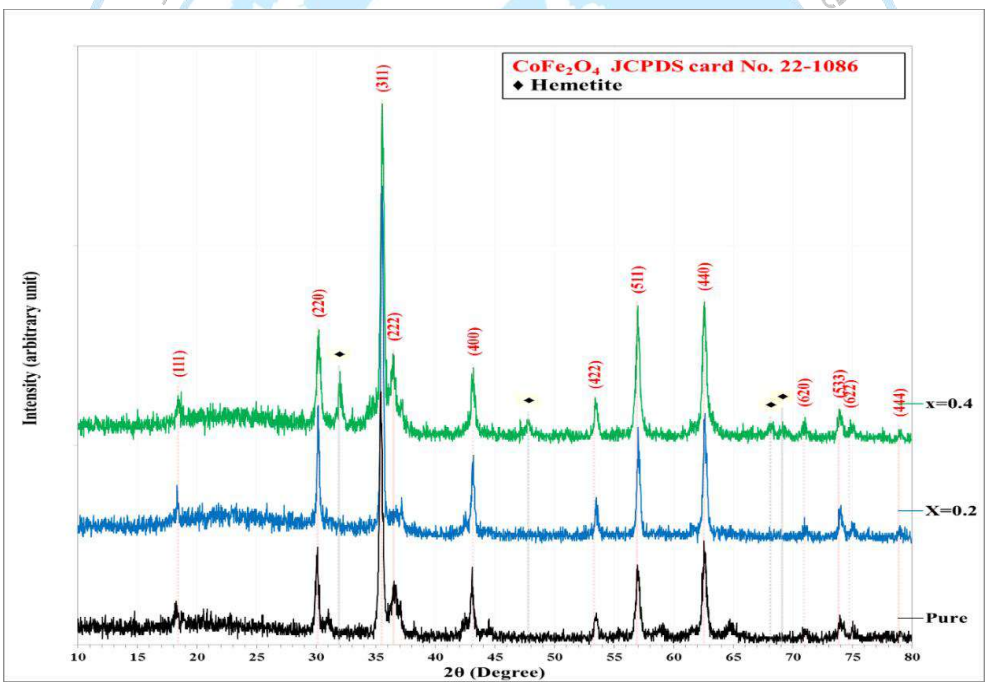

Figure 3: XRD patterns for $Co_{1-x}Ni_xFe_2O_4$ powders prepared at different ratios.

The inter-planer distances of the crystal layers (d_{hkl}) were calculated using the Bragg equation, while the crystal size was estimated using Scherrer equation depending on the broadening of the diffraction lines at the half maxima (FWHM), as shown in Table 2. The crystal size increases at the middle ratio (X=0.2 Ni), while it decreases at the higher Ni substitution. The average

crystallite sizes for $CoFe_2O_4$, $Co_{0.8}Ni_{0.2}Fe_2O_4$, and $Co_{0.6}Ni_{0.4}Fe_2O_4$ samples were 22.6, 26.6, and 25.2 nm, respectively, which are in agreement with the peak broadening.

Table 2: XRD parameters for $Co_{1-x}Ni_xFe_2O_4$ powders prepared at different ratios

Sample	2θ (Deg.)	FWHM (Deg.)	d_{hkl} (Å)	D (nm)	hkl
X=0	18.2650	0.3752	4.8533	21.5	(111)
	30.0835	0.3484	2.9681	23.6	(220)
	35.4434	0.4288	2.5306	19.5	(311)
	36.5690	0.4556	2.4553	18.4	(222)
	43.0812	0.3484	2.0980	24.5	(400)
	53.4526	0.3752	1.7128	23.7	(422)
	56.9633	0.3484	1.6153	26.0	(511)
	62.5912	0.4020	1.4829	23.1	(440)
	71.0062	0.5092	1.3264	19.2	(620)
	74.0613	0.5360	1.2791	18.6	(533)
	75.0529	0.3216	1.2646	31.2	(622)
X=0.2	18.3346	0.2412	4.8350	33.4	(111)
	30.1531	0.2680	2.9614	30.7	(220)
	35.5130	0.2948	2.5258	28.3	(311)
	36.5850	0.4556	2.4542	18.4	(222)
	43.1508	0.3216	2.0948	26.6	(400)
	53.4954	0.3216	1.7115	27.7	(422)
	57.0597	0.3484	1.6128	26.0	(511)
	62.5804	0.4020	1.4831	23.1	(440)
	70.9686	0.4288	1.3270	22.8	(620)
	74.0237	0.3752	1.2796	26.5	(533)
	74.9349	0.4288	1.2663	23.3	(622)
	78.9280	0.3216	1.2119	32.0	(444)
X=0.4	18.4346	0.3487	4.8090	23.1	(111)
	30.1995	0.3483	2.9570	23.6	(220)
	35.5326	0.3484	2.5245	24.0	(311)
	36.4170	0.3484	2.4652	24.0	(222)
	43.1168	0.3484	2.0963	24.5	(400)
	53.4346	0.2948	1.7133	30.2	(422)
	56.9721	0.4020	1.6151	22.5	(511)
	62.5464	0.4020	1.4839	23.1	(440)
	70.9346	0.3752	1.3276	26.0	(620)
	73.8825	0.4020	1.2817	24.7	(533)
	74.8741	0.3752	1.2672	26.7	(622)
	79.0280	0.3484	1.2107	29.6	(444)

Depending on the following equation for the cubic crystalline structure [9]:

Diyala Journal for Pure Science

Synthesis and Characterization of Magnetic (Co-Ni-Fe2O4) Nano Ferrite for Biomedical Application

Marwa H. Sabbar, T. H. Mubarak and Nada S. Ahmad

$$d_{hkl} = \frac{a}{\sqrt{h^2+k^2+l^2}} \quad \text{.....(2)}$$

The lattice constant (a) was calculated from the slope of the straight line for the relationship between the values of d_{hkl} against $1/\sqrt{h^2+k^2+l^2}$, for $Co_{1-x}Ni_xFe_2O_4$ powders prepared at different ratios as shown in Figure 4.

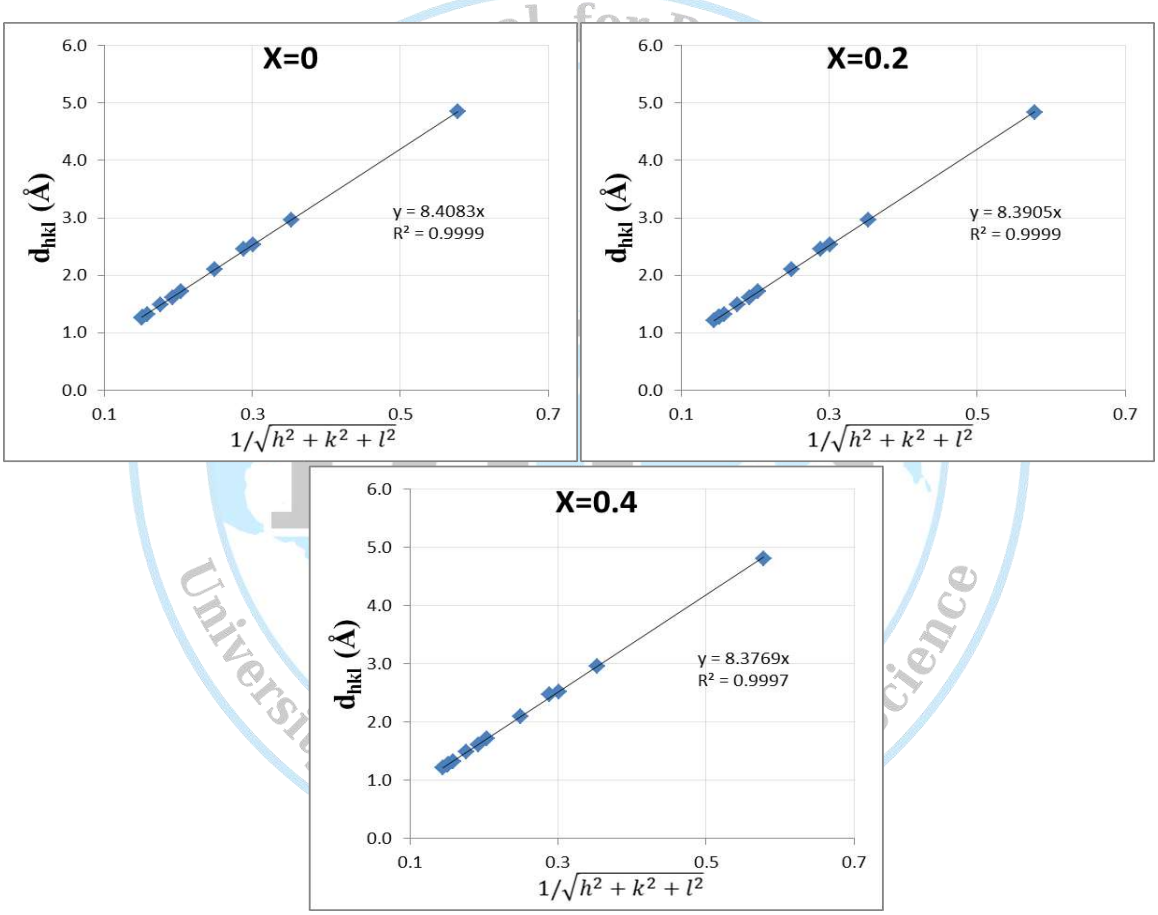

Figure 4: Calculation of lattice constant for spinal structure of $Co_{1-x}Ni_xFe_2O_4$ powders prepared at different ratios

As shown in Table 4, the lattice parameter of the prepared cobalt ferrites was reduced linearly with the increase of Ni content from 8.408 Å to 8.377 Å. The reported lattice parameters for spinal $CoFe_2O_4$ is 8.376 Å and for spinal $NiFe_2O_4$ is 8.337 Å, while for $Co_{1-x}Ni_xFe_2O_4$ between

these values [7]. The determined lattice constant values have the same behavior as it decreases with the increase of the compensated nickel percentage, but it has slightly larger values than the previously calculated values. It may be due to crystal defects as a result of presence a secondary phase that causes strain in lattice [7].

The lattice density (ρ_x) of $Co_{1-x}Ni_xFe_2O_4$ at different Ni ratio was calculated by Smith and Wijn formula [10]

$$\boldsymbol{\rho_x = \frac{n\,M_w}{N_A\,a^3}} \quad \textbf{.....(3)}$$

where N_A is the Avogadro's number, n denotes number of molecules present in the unit cell (n = 8 for spinal structure) [10] and M_w represents the molecular weight (equal the summation of ratio of each element product their atomic weight).

The variation of distance between magnetic ions in the tetrahedral A-site (L_A) and the distance between magnetic ions in the octahedral B-site (L_B) were calculated using the relations [11]:

$$\boldsymbol{L_A = \frac{\sqrt{3}a}{4}} \quad \textbf{.....(4)}$$

$$\boldsymbol{L_B = \frac{\sqrt{3}a}{2}} \quad \textbf{.....(5)}$$

The calculated values of lattice constant (a), lattice volume(V), lattice density (ρ_x), L_A, and L_B are listed in Table 3. The revealed sensitivity of the ion jump lengths (L_A and L_B) on the amount of substitution of Ni instead of Co in the ferrite structure was attributed to the ionic radii mismatch variation [11]. Both L_A and L_B were reduced with increasing the Ni substitution.

Table 3: lattice constant (a), lattice volume (V), lattice density (ρ_x), and ion jump lengths (L_A, L_B) for $Co_{1-x}Ni_xFe_2O_4$ powders prepared at different ratios.

X	a (Å)	V(Å^3)	ρ_x(gm/cm^3)	L_A	L_B
0	8.4083	594.463	5.243	3.641	7.282
0.2	8.3905	590.695	5.276	3.633	7.266
0.4	8.3769	587.828	5.300	3.627	7.255

2. X-ray Diffraction (XRD) patterns of Co-Ni-Fe_2O_4 for PLD method

Figure 5 displays the XRD patterns for $Co_{1-x}Ni_xFe_2O_4$ thin films deposited on glass slides by pulsed laser from pellet of different Ni substitution ratios. Also, Face-center cubic structure for the all patterns with nearly same peaks of Spinal phase appeared in the powder samples but with less crystallinity. Additional miner phases of Hematite (Fe_2O_3) and Magnetite (Fe_3O_4) appeared in thin film samples [7].

All peaks have broad feature compared with co-precipitation indicate on nano-crystalline structure. The higher crystallinity appeared at 0.2 Ni substitution ratio. Also, increasing the substitution levels of Ni instead of Co into the spinal ferrite structures cause to slightly shifts in the peaks locations toward higher diffraction angles [9].

The inter-planer distances were calculated using the Bragg equation, while the crystal size was estimated using Scherrer equation according to the diffraction lines broadening. As shown in Table 4., the average crystal size of the films prepared by pulsed laser was much smaller than that of the powder samples, where the average crystallite sizes for $CoFe_2O_4$, $Co_{0.8}Ni_{0.2}Fe_2O_4$, and $Co_{0.6}Ni_{0.4}Fe_2O_4$ samples measured using the Scherrer equation were 13.7, 13.4, and 13.9 nm.

Diyala Journal for Pure Science

Synthesis and Characterization of Magnetic (Co-Ni-Fe2O4) Nano Ferrite for Biomedical Application

Marwa H. Sabbar, T. H. Mubarak and Nada S. Ahmad

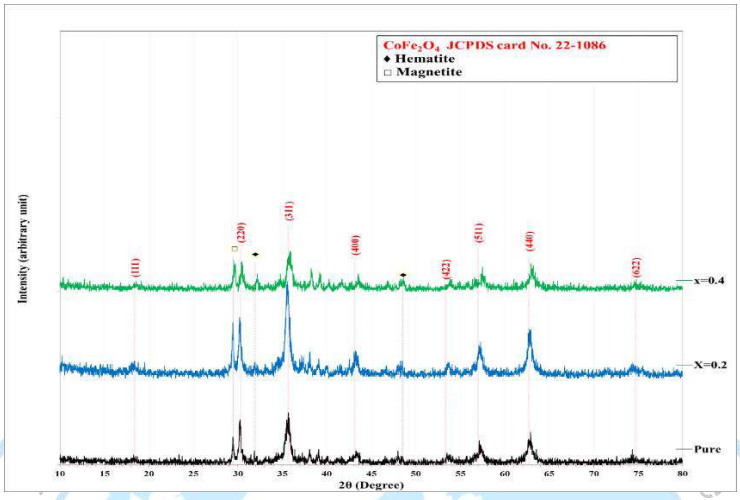

Figure 5: XRD patterns for $Co_{1-x}Ni_xFe_2O_4$ thin films deposited at different ratios

Table 4: XRD parameters for $Co_{1-x}Ni_xFe_2O_4$ thin films prepared at different ratios

Sample	2θ (Deg.)	FWHM (Deg.)	d_{hkl} (Å)	D (nm)	hkl
X=0	18.3571	0.6313	4.8291	12.8	(111)
	30.2810	0.3507	2.9492	23.5	(220)
	35.6818	0.7014	2.5142	11.9	(311)
	43.3271	0.7014	2.0867	12.2	(400)
	53.6377	0.7716	1.7073	11.5	(422)
	57.2148	0.7715	1.6088	11.7	(511)
	62.7559	0.7014	1.4794	13.3	(440)
	74.3291	0.7716	1.2751	12.9	(622)
X=0.2	18.4168	0.7716	4.8136	10.4	(111)
	30.2705	0.4209	2.9502	19.6	(220)
	35.5311	0.5612	2.5246	14.9	(311)
	43.2465	0.6312	2.0904	13.5	(400)
	53.6974	0.7014	1.7056	12.7	(422)
	57.1343	0.6313	1.6109	14.3	(511)
	62.8156	0.7014	1.4781	13.3	(440)
	74.4589	1.1924	1.2732	8.4	(622)
X=0.4	18.5571	0.6312	4.7775	12.8	(111)
	30.4810	0.4910	2.9303	16.8	(220)
	35.9519	0.7014	2.4960	11.9	(311)
	43.5271	0.4910	2.0775	17.4	(400)
	53.9078	0.5611	1.6994	15.9	(422)
	57.4850	0.7015	1.6019	12.9	(511)
	63.0261	0.9118	1.4737	10.2	(440)
	74.6693	0.7716	1.2701	13.0	(622)

Diyala Journal for Pure Science

Synthesis and Characterization of Magnetic (Co-Ni-Fe2O4) Nano Ferrite for Biomedical Application

Marwa H. Sabbar, T. H. Mubarak and Nada S. Ahmad

The lattice constant (a) was calculated from the slope of the straight line for the relationship between the values of d_{hkl} against $1/\sqrt{h^2+k^2+l^2}$, for $Co_{1-x}Ni_xFe_2O_4$ thin films prepared at different Ni content as shown in Figure 6.

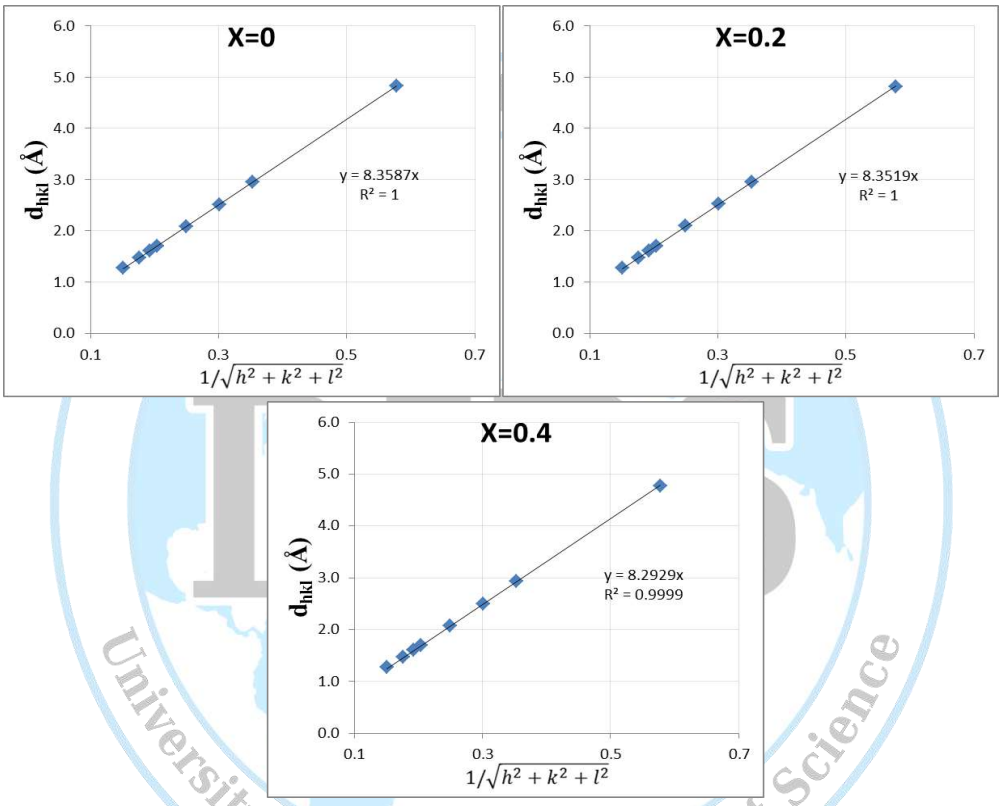

Figure 6: Calculation of lattice constant for spinal structure of $Co_{1-x}Ni_xFe_2O_4$ thin films deposited at different ratios

As shown in Table 5, the lattice parameter of the prepared cobalt ferrites was reduced from 8.3587 Å to 8.2929 Å with increasing the Ni substitution from 0 to 0.4. The determined lattice constant values for the thin film samples have the same behavior as highlighted of the substituted Ni ratio as in powder samples. The variation of ion jumps lengths (L_A and L_B) were calculated using the relations 4.3 and 4.4. The calculated values of a, V, ρ_x, L_A, and L_B are listed in Table 5. It seems that both L_A and L_B were reduced with increasing the Ni substitution.

Synthesis and Characterization of Magnetic (Co-Ni-Fe2O4) Nano Ferrite for Biomedical Application

Marwa H. Sabbar, T. H. Mubarak and Nada S. Ahmad

Table 5: lattice constant (a), lattice volume (V), lattice density (ρ_x), and ion jump lengths (LA, LB) for $Co_{1-x}Ni_xFe_2O_4$ thin films prepared at different ratios

X	a (Å)	V(Å^3)	ρ(gm/cm^3)	L_A	L_B
0	8.3587	584.005	5.337	3.619	7.239
0.2	8.3519	582.580	5.349	3.616	7.233
0.4	8.2929	570.321	5.463	3.591	7.182

3. Vibrating Sample Magnetometer (VSM) of $Co-Ni-Fe_2O_4$ for Co-precipitation method

The magnetic property test for $Co_{1-x}Ni_xFe_2O_4$ ferrite powders, prepared by co-precipitation method at different Ni-Co substitution ratios, tested using vibrating sample magnetometer (VSM) were shown in Figure 7. All samples showed a typical S-shaped hysteresis ring. The hysteresis loop area decreased in with increasing the Ni ratio.

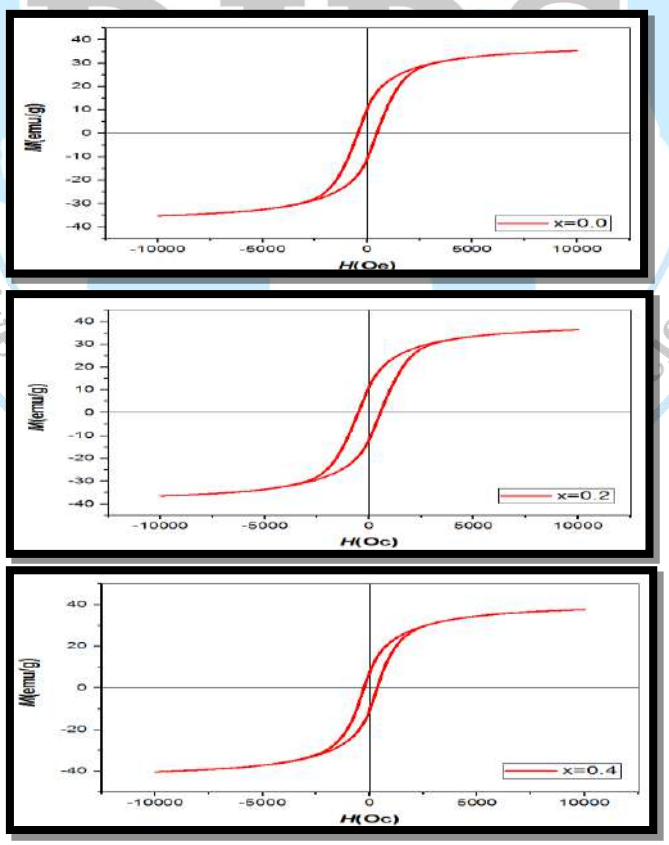

Figure 7: The magneto-hysteresis loop for $Co_{1-x}Ni_xFe_2O_4$ powders prepared at different ratios.

Figure 8. illustrate the variation of residual magnetization (Mr) and the coercive field (Hc) for Co1-xNixFe2O4 with Ni ratio for powder and thin films samples for respectively. Table 7 shows the VSM parameters for the powder samples.

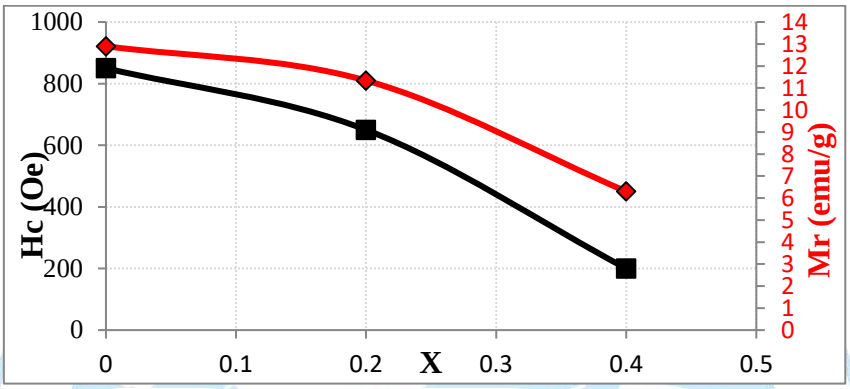

Figure 8: Variation of residual magnetization and coercive field for $Co_{1-x}Ni_xFe_2O_4$ powder at different ratios.

Table 7: Magnetization parameters for $Co_{1-x}Ni_xFe_2O_4$ powder at different ratios.

X	M_r (emu/g)	H_c (Oe)	M_s (emu/g)
0	12.9	850	35.5
0.2	11.3	650	34.8
0.4	6.3	200	34.3

4. Vibrating Sample Magnetometer (VSM) of Co-Ni-Fe_2O_4 for PLD method

Figure 9. shows the VSM test for $Co_{1-x}Ni_xFe_2O_4$ ferrite thin film, prepared by PLD at different Ni contents on glass slides. Also, typical hysteresis loop appeared for the thin film samples but with less area. Similarly, the hysteresis loop area decreased with increasing the Ni ratio. The coercive field (Hc), residual magnetization (Mr), saturation magnetization (Ms), for thin films samples, were extrapolated from the two figures and included in Table 8.

Diyala Journal for Pure Science

Synthesis and Characterization of Magnetic (Co-Ni-Fe2O4) Nano Ferrite for Biomedical Application

Marwa H. Sabbar, T. H. Mubarak and Nada S. Ahmad

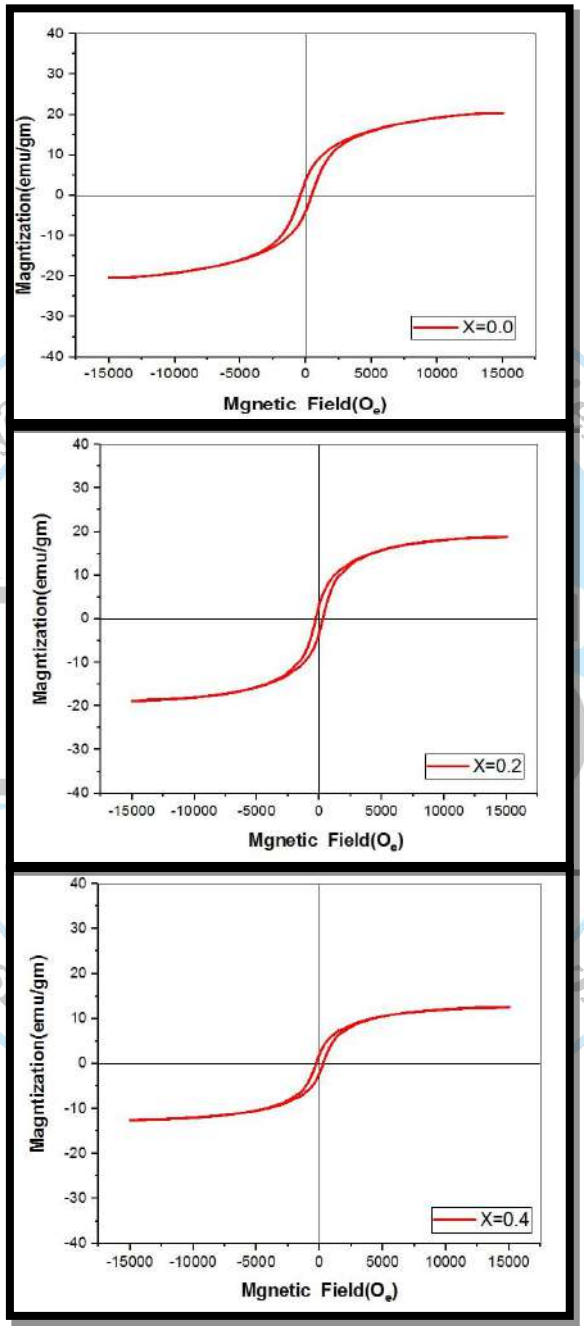

Figure 9: The magneto-hysteresis loop for $Co_{1-x}Ni_xFe_2O_4$ thin films deposited at different ratios.

Table 8: Magnetization parameters for $Co_{1-x}Ni_xFe_2O_4$ thin films at different ratios.

X	M_r (emu/g)	H_c (Oe)	M_s (emu/g)
0	2.13	450	12.5
0.2	3.19	285	18.9
0.4	3.82	220	20.0

Figure 10. illustrates the variation of residual magnetization (M_r) and the coercive field (H_c) for $Co_{1-x}Ni_xFe_2O_4$ with the Ni ratio for thin films samples.

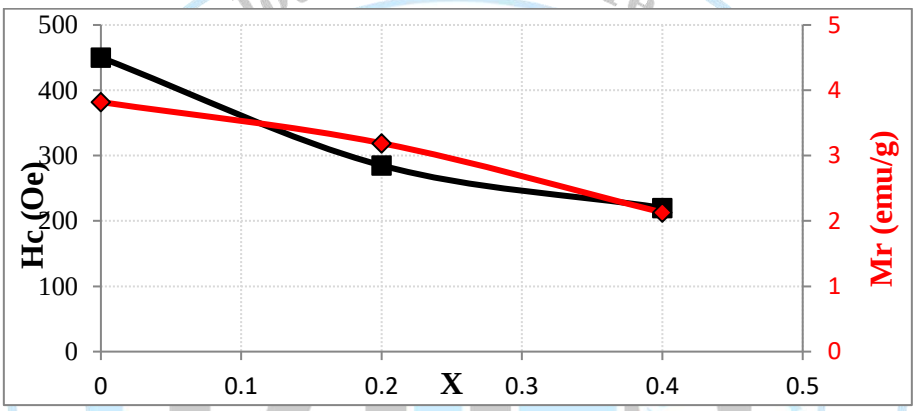

Figure 10: variation of residual magnetization and coercive field for $Co_{1-x}Ni_xFe_2O_4$ thin films at different ratios

5. Antibacterial activity

The antibacterial potential of the prepared $Co_{1-x}Ni_xFe_2O_4$ powder and thin films was investigated against Gram's negative (*E.coli*) and Gram's positive (*S.aureus*) bacterial strains (the most prevalent clinically resistant pathogenic bacteria) using agar well diffusion assay. About 20 mL of on Muller–Hinton (MH) agar was aseptically poured into sterile Petri dishes. The bacterial species were collected from their stock cultures using a sterile wire loop. After culturing the organisms, 6 mm-diameter wells were bored on the agar plates using of a sterile tip. Into the bored wells, different concentrations of the sample (100%, 75%, 50%, and 25%) were used. The cultured plates containing the $Co_{1-x}Ni_xFe_2O_4$ samples and the test organisms were incubated overnight at 37 °C before measuring and recording the average the zones of inhibition diameter.

Diyala Journal for Pure Science

Marwa H. Sabbar, T. H. Mubarak and Nada S. Ahmad

5.1 Antibacterial activity for *E.Coli*.

Figure 11. shows antibacterial activity test of $Co_{1-x}Ni_xFe_2O_4$ powders at different Ni content against *E.Coli*. The highest antibacterial activity appeared for the sample prepared for the 0.4 Ni ratio sample with 30 mm inhibition zone diameter. Figure 12. shows antibacterial activity test of $Co_{1-x}Ni_xFe_2O_4$ thin films at different Ni content against *E.Coli*. Also, the highest antibacterial activity appeared for the highest Ni ratio sample with 30 mm inhibition zone diameter and few reduced to 27 mm when diluted the sample to 25%.

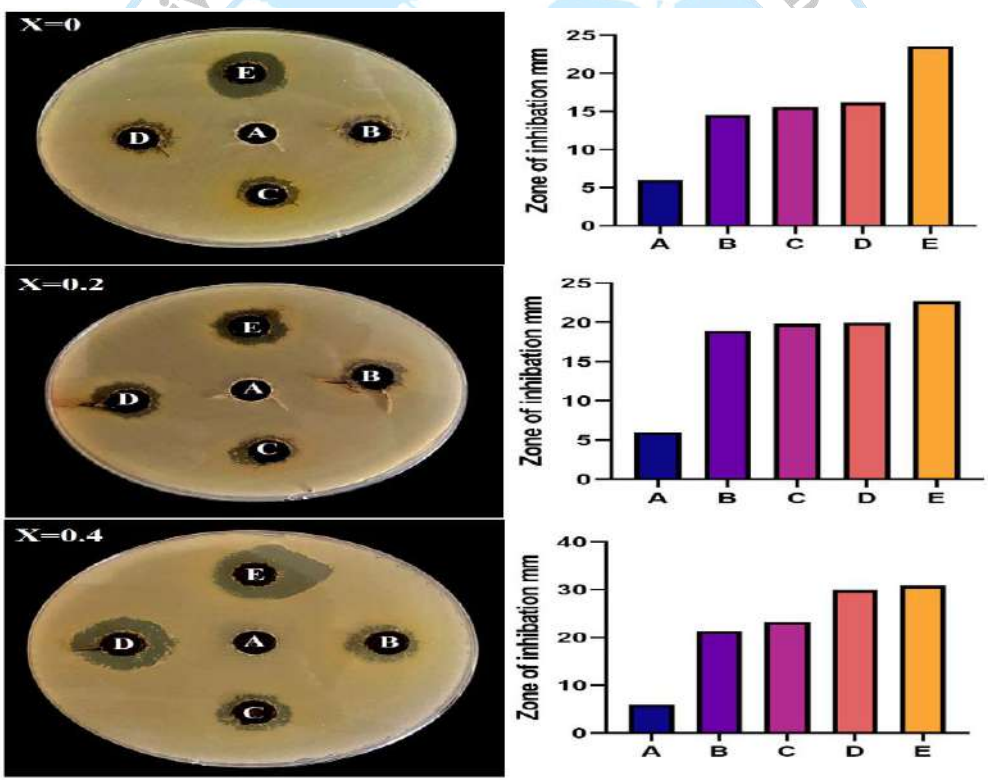

Figure 11: Antibacterial activity of $Co_{1-x}Ni_xFe_2O_4$ thin powder at different Ni content against *E.Coli*.. A, control. B, 25%. C, 50%. D, 75%. E, 100%

Diyala Journal for Pure Science

Synthesis and Characterization of Magnetic (Co-Ni-Fe2O4) Nano Ferrite for Biomedical Application

Marwa H. Sabbar, T. H. Mubarak and Nada S. Ahmad

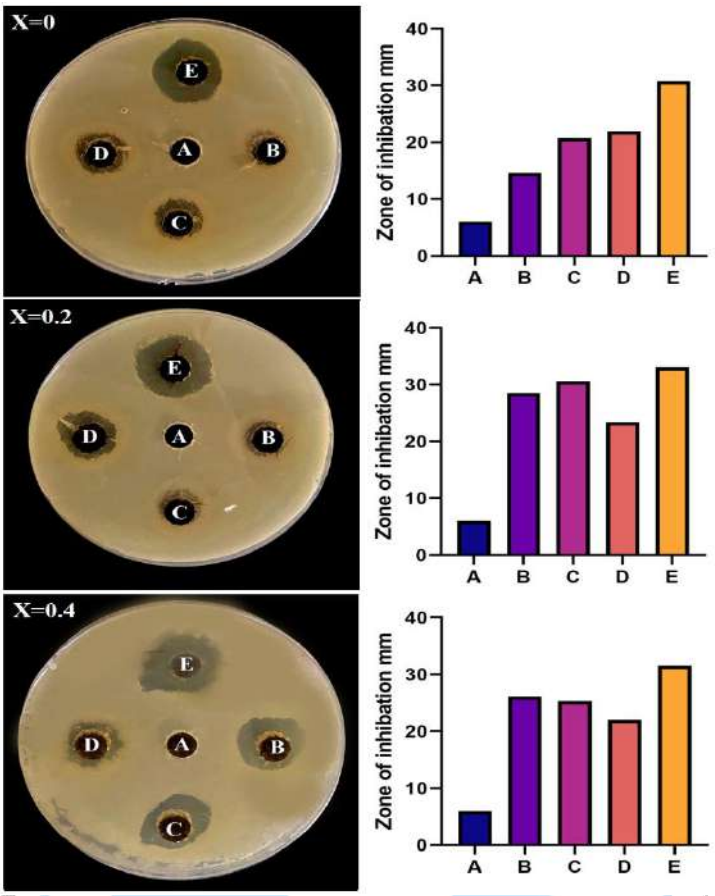

Figure 12: Antibacterial activity of $Co_{1-x}Ni_xFe_2O_4$ thin films at different Ni content against *E.Coli*.. A, control. B, 25%. C, 50%. D, 75%. E, 100%

5.2 Antibacterial activity for *S. aureus.*

Figure 13. displays the antibacterial potential test for the $Co_{1-x}Ni_xFe_2O_4$ powder at different Ni content against ***S. aureus.*** bacteria. The highest antibacterial activity appeared for the $CoFe_2O_4$ sample with 33 mm inhibition zone diameter for the100% concentration, and reduced to 27 mm inhibition zone for 25% concentration. Figure 14. shows antibacterial activity test of $Co_{1-x}Ni_xFe_2O_4$ thin films at different Ni content against *S.aureus*. The highest antibacterial activity appeared for the $CoFe_2O_4$ sample with 32 mm inhibition zone inhibition zone diameter and reduced to 22 mm when diluted the sample to 25%.

Diyala Journal for Pure Science

Synthesis and Characterization of Magnetic (Co-Ni-Fe2O4) Nano Ferrite for Biomedical Application

Marwa H. Sabbar, T. H. Mubarak and Nada S. Ahmad

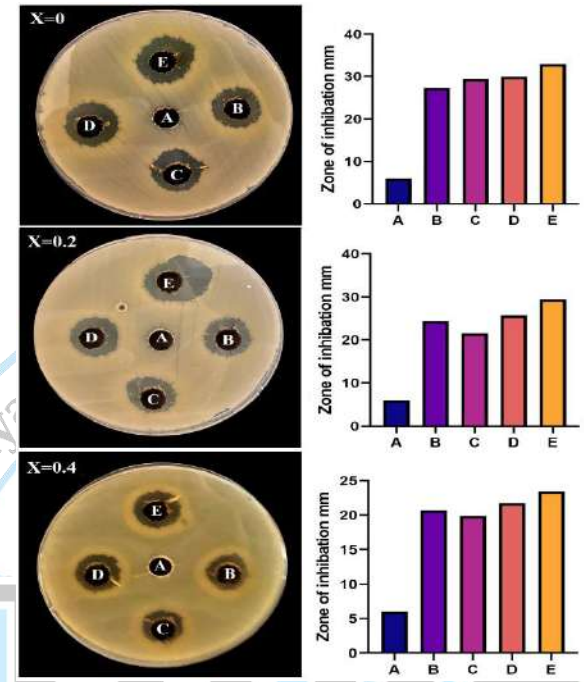

Figure 13: Antibacterial activity of $Co_{1-x}Ni_xFe_2O_4$ powders at different Ni content against *S. aureus.* A, control. B, 25%. C, 50%. D, 75%. E, 100%.

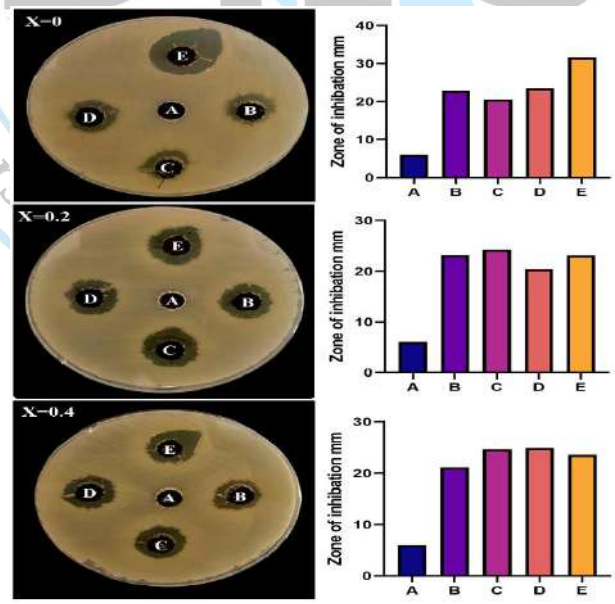

Figure 14: Antibacterial activity of $Co_{1-x}Ni_xFe_2O_4$ thin films at different Ni content against S. *aureus.* A, control. B, 25%. C, 50%. D, 75%. E, 100%.

The results demonstrate that the better inhibition of the bacterial growth for Gram-positive compared with the Gram-negative. This result may be due to the variation in bacterial wall structure. Gram-negative bacteria has a lipid-bilayer membrane, which gives them higher resistance to NPs [15].

The examination showed that all samples had good antibacterial activity. The bacteria-killing process can be explained by different mechanisms: The antibacterial activity of metal ions (Ni^{2+}, Co^{2+}, and Fe^{3+}) liberated from samples that penetrate the bacteria cell and have toxic nature, oxidative stress, damage to cell membranes after contact with their surface, proteolysis, or the combination of all these factors [13], [16].

The created nanoparticles candidate for use in drug delivery, as its magnetic and antibacterial properties [14]. While, the resultant magnetic thin film with antibacterial behavior is candidate for exploring applications in micro-electromagnetic systems such as micropumps, and robots [17].

Conclusions

- The XRD patterns confirm the cubic spinel structure. Same peaks of Spinal phase appeared in thin films samples but with less crystallinity. Broad feature for diffraction lines in thin films (compared with co-precipitation) indicate on Nano-crystalline structure. The crystalline size measured using the Scherrer equation for thin film less than for powder samples
- The magnetic properties have a good correlation with the structural parameters of the spinal structure.
- The samples show good antibacterial potential, especially against gram-positive strain bacteria.

Synthesis and Characterization of Magnetic (Co-Ni-Fe2O4) Nano Ferrite for Biomedical Application

Marwa H. Sabbar, T. H. Mubarak and Nada S. Ahmad

References

1. M. J. Iqbal, Z. Ahmad, Journal of Power Sources, 179(2), 763-769(2008)
2. C. S. Kim, Y. S. Yi, K. T. Park, H. Namgung, J. G. Lee, Journal of applied physics, 85(8), 5223-5225(1999)
3. S. Singh, N. K. Ralhan, R. K. Kotnal, K. C. Verma, Indian J. Pure Appl. Phys. 50, 739–743(2012)
4. Nga H. N. Do, T. P. Luu, Q. B. Thai, D. K. Le, Ngoc Do Quyen Chau, Son T. Nguyen, Phung K. Le, N. Phan-Thien, H. M. Duong, Materials Technology, 35(11-12), 807-814(2019)
5. D. M. S.A. Salem, The Egyptian Journal of Aquatic Research,45(3), 197-204(2019)
6. M. A. Abid, D. A. Kadhim, Materials Technology, 1-10(2021)
7. J.-L. Ortiz-Quiñonez, U. Pal, M. S. Villanueva, ACS Omega, 3, 14986−15001(2018)
8. F. Tudorache, P. D. Popa, M. Dobromir, F. Iacomi, Mater. Sci. Eng. B, 178, 1334– 1338 (2013)
9. K. Jalaiah, K. C. Mouli, K. V. Babu, R.V. Krishnaiah, J. Sci. Adv. Mater. Devices, 4, 310–318(2019)
10. A. R. Chavan, R. R. Chilwar, P. B. Kharat, K. M. Jadhav, J. Supercond. Nov. Magn., 31, 2949–2958(2018)
11. R. Tiwaria, M. De, H. S. Tewari, S.K. Ghoshal, Results Phys., 16, 102916(2020)
12. O. Abd-Elkader, A. M. Al-Enizi, S. F. Shaikh, M. Ubaidullah, M. O. Abdelkader, N. Y. Mostafa, Cryst. Artic.,12, 393(2022)
13. S. Munir, M. F. Warsi, S. H. Sonia Zulfiqar b, Imtisal Aymana, I. A. Alsafari, P. O. Agboola, and I. Shakir, J. Saudi Chem. Soc., 25, 101388(2021)
14. R. S. Chaughule R. V. Ramanujan, in Nanoparticles: Synthesis, Characterization and Applications, American Scientific Publishers, 1–20(2010)
15. M. Kooti, S. Gharineh, M. Mehrkhah, A. Shaker, H. Motamedi, Chem. Eng. J., 259, 34–42(2015)
16. K. L. Rincón-Granados, A. R. Vázquez-Olmos, A.-P. R.- Hernández, A. Vega-Jiménez, F. Ruiz, and V. G.-F. L.-A. Ximénez-Fyvie, Materialia, 15, 100955(2021)
17. D. Ficai, Micromachines,13(3), 351(2022)